

This is the accepted manuscript made available via CHORUS. The article has been published as:

Magnetic dilution and domain selection in the XY pyrochlore antiferromagnet $\text{Er}_{\{2\}}\text{Ti}_{\{2\}}\text{O}_{\{7\}}$

J. Gaudet, A. M. Hallas, D. D. Maharaj, C. R. C. Buhariwalla, E. Kermarrec, N. P. Butch, T. J. S. Munsie, H. A. Dabkowska, G. M. Luke, and B. D. Gaulin

Phys. Rev. B **94**, 060407 — Published 15 August 2016

DOI: [10.1103/PhysRevB.94.060407](https://doi.org/10.1103/PhysRevB.94.060407)

Magnetic dilution and domain selection in the XY pyrochlore antiferromagnet $\text{Er}_2\text{Ti}_2\text{O}_7$

J. Gaudet,¹ A. M. Hallas,¹ D. D. Maharaj,¹ C. R. C. Buhariwalla,¹ E. Kermarrec,¹
N. P. Butch,² T. J. S. Munsie,¹ H. A. Dabkowska,³ G. M. Luke,^{1,4} and B. D. Gaulin^{1,3,4}

¹*Department of Physics and Astronomy, McMaster University, Hamilton, ON L8S 4M1, Canada*

²*NIST Centre for Neutron Research, Gaithersburg Maryland USA*

³*Brockhouse Institute for Materials Research, Hamilton, ON L8S 4M1, Canada*

⁴*Canadian Institute for Advanced Research, 180 Dundas Street West, Toronto, Ontario M5G 1Z8, Canada*

(Dated: July 25, 2016)

Below $T_N = 1.1$ K, the XY pyrochlore $\text{Er}_2\text{Ti}_2\text{O}_7$ orders into a $k = 0$ non-collinear, antiferromagnetic structure referred to as the ψ_2 state. The magnetic order in $\text{Er}_2\text{Ti}_2\text{O}_7$ is known to obey conventional three dimensional (3D) percolation in the presence of magnetic dilution, and in that sense is robust to disorder. Recently, however, two theoretical studies have predicted that the ψ_2 structure should be unstable to the formation of a related ψ_3 magnetic structure in the presence of magnetic vacancies. To investigate these theories, we have carried out systematic elastic and inelastic neutron scattering studies of three single crystals of $\text{Er}_{2-x}\text{Y}_x\text{Ti}_2\text{O}_7$ with $x = 0$ (pure), 0.2 (10%-Y) and 0.4 (20%-Y), where magnetic Er^{3+} is substituted by non-magnetic Y^{3+} . We find that the predicted change in ground state selection, from ψ_2 to ψ_3 , does not occur, and yet the ground state is still significantly affected by magnetic dilution. The characteristic domain selection associated with the ψ_2 state, and the corresponding energy gap separating ψ_2 from ψ_3 , vanish for Y^{3+} substitutions between 10%-Y and 20%-Y, far removed from the 3D percolation threshold of $\sim 60\%$ -Y. The resulting ground state for $\text{Er}_2\text{Ti}_2\text{O}_7$ with magnetic dilutions from 20%-Y up to the percolation threshold is naturally interpreted as a frozen mosaic of ψ_2 and ψ_3 domains.

PACS numbers: 75.25.-j, 75.10.Kt, 75.40.Gb, 71.70.Ch

The network of corner-sharing tetrahedra that make up the pyrochlore lattice is one of the canonical architectures for geometrical frustration in three dimensions [1]. In the pyrochlore magnets with chemical composition $A_2B_2O_7$, each of the A^{3+} and B^{4+} sublattices independently form such a network, that can be decorated by many ions. The rare earth titanate family, $R_2\text{Ti}_2\text{O}_7$, which features a single magnetic R^{3+} site and non-magnetic Ti^{4+} on the B -site, has been of specific interest. This family displays a great variety of exotic magnetic ground states, including classical [2–4] and quantum spin ice [5–8], as well as spin liquid states [9–11]. Such exotic states arise from different combinations of magnetic anisotropies with differing exchange and dipolar interactions, depending on the nature of the R^{3+} magnetic ion.

Much current interest is focused on the XY antiferromagnetic pyrochlore $\text{Er}_2\text{Ti}_2\text{O}_7$, which displays an antiferromagnetic Curie-Weiss susceptibility with $\theta_{CW} = -22$ K [12]. Crystal field effects on Er^{3+} in this environment give rise to a g -tensor with XY anisotropy [13–15]. In contrast to the exotic ground states displayed by other members of the $R_2\text{Ti}_2\text{O}_7$ family, $\text{Er}_2\text{Ti}_2\text{O}_7$ has a rather conventional $k = 0$, Γ_5 antiferromagnetic ground state below $T_N = 1.1$ K [12, 16–19]. Γ_5 is made up of two basis vectors, referred to as ψ_2 and ψ_3 , and sophisticated magnetic crystallography was used to identify the ordered structure in $\text{Er}_2\text{Ti}_2\text{O}_7$ as ψ_2 [16]. The microscopic spin Hamiltonian for $\text{Er}_2\text{Ti}_2\text{O}_7$ was determined through measurements of the spin wave dispersions within its field polarized state [20, 21]. This work,

amongst others [12, 22, 23], has provided an explanation for the selection of ψ_2 within the Γ_5 manifold in terms of a quantum order-by-disorder mechanism. The order-by-disorder scenario has been further strengthened by works showing that thermal fluctuations also select ψ_2 over ψ_3 [24–27]. A spin wave gap of 0.053 ± 0.006 meV has been successfully measured in $\text{Er}_2\text{Ti}_2\text{O}_7$, consistent with the order-by-disorder mechanism [28]. Recently, there has been a proposal that the selection of the ψ_2 ordered state could also occur via higher multipolar interactions, originating from virtual crystal field transitions [21, 29].

The phase transition to the ψ_2 antiferromagnetic ordered state in $\text{Er}_2\text{Ti}_2\text{O}_7$ is unusual amongst the $R_2\text{Ti}_2\text{O}_7$ family by virtue of how conventional it is. In contrast to $\text{Yb}_2\text{Ti}_2\text{O}_7$ [30–32] and $\text{Tb}_2\text{Ti}_2\text{O}_7$ [33, 34], there appears to be no sample dependence to its low temperature phase diagram. Also, systematic studies of magnetic dilution at the rare earth site in $\text{Er}_2\text{Ti}_2\text{O}_7$ are consistent with three dimensional (3D) percolation theory [35]. It was therefore surprising that two recent, independent theoretical works predicted that, upon magnetic dilution, the ψ_2 ground state selection in $\text{Er}_2\text{Ti}_2\text{O}_7$ should be unstable to the selection of its ψ_3 partner within the Γ_5 manifold [36, 37].

Such a possible ψ_2 to ψ_3 phase transition upon magnetic dilution in $\text{Er}_2\text{Ti}_2\text{O}_7$ has yet to be explored experimentally and is the topic of this manuscript. The phase transition between ψ_2 and ψ_3 in $\text{Er}_2\text{Ti}_2\text{O}_7$ is predicted to occur near a critical dilution of $\sim 10\%$ [36, 37]. As Y^{3+} is non-magnetic and comparable in size to Er^{3+} , it is an

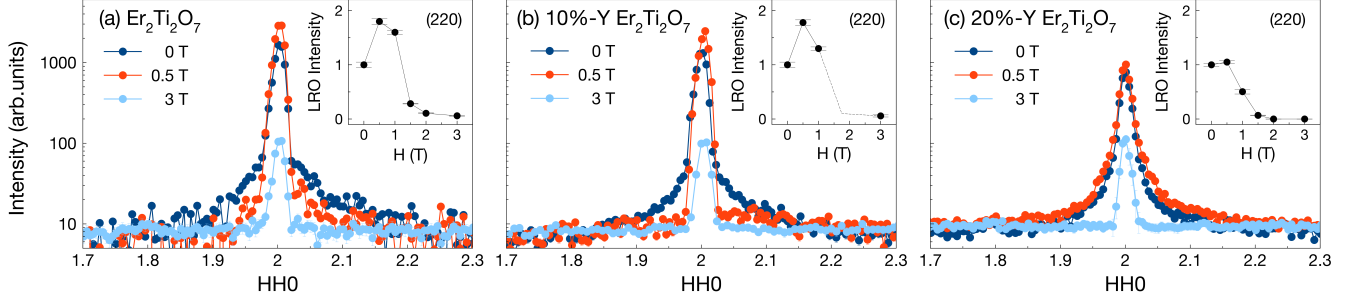


FIG. 1. Magnetic Bragg peak intensity for $Q = (220)$ as a function of field for the pure, 10%-Y and 20%-Y diluted samples of $\text{Er}_{2-x}\text{Y}_x\text{Ti}_2\text{O}_7$. The elastic scattering was isolated by integrating from -0.2 to 0.2 in the $[00L]$ direction and from -0.1 to 0.1 meV in energy transfer. The insets show the integrated intensity of the long range ordered component of the scattering for each of the three samples. Examples of the fits used to obtain these intensities are shown in Fig.1 of the Supplemental Material. The dashed line in the inset of (b) indicates the expected behavior for the 10%-Y sample at 1.75 T.

	T_N (K)	θ_{CW} (K)	$\mu_{\text{eff}}/\text{Er}^{3+}$
$\text{Er}_2\text{Ti}_2\text{O}_7$ (0%)	1.1(1)	$-18.0(2)$	$9.555(4) \mu_B$
$\text{Er}_{1.8}\text{Y}_{0.2}\text{Ti}_2\text{O}_7$ (10%)	1.04(5)	$-17.2(3)$	$8.965(7) \mu_B$
$\text{Er}_{1.6}\text{Y}_{0.4}\text{Ti}_2\text{O}_7$ (20%)	0.74(8)	$-17.7(3)$	$8.523(6) \mu_B$

TABLE I. Summary of the dc susceptibility measurements performed on each of $\text{Er}_{2-x}\text{Y}_x\text{Ti}_2\text{O}_7$ with 0%, 10% and 20% yttrium-doped samples. The full data are shown in the Supplemental Material.

ideal ion to employ for magnetic dilution studies. Hence, we have grown single crystal samples of $\text{Er}_{2-x}\text{Y}_x\text{Ti}_2\text{O}_7$ with $x = 0$ (pure), 0.2 (10%-Y) and 0.4 (20%-Y) to investigate a possible change in the magnetic ground state. We performed time-of-flight inelastic neutron scattering measurements on these three single crystals at various temperatures and magnetic fields. Our results show that the signature for ψ_2 long range magnetic order disappears upon dilution, but without the system ordering into ψ_3 . Instead, we observe a softening of the zero field, low energy excitations at the (220) ordering wavevector, consistent with a closing of the spin gap. At a relatively high level of magnetic dilution, on the order of 20%-Y, the system cannot globally select the ψ_2 state over ψ_3 , and we suggest that it forms a frozen mosaic of both ψ_2 and ψ_3 domains.

The three $\text{Er}_{2-x}\text{Y}_x\text{Ti}_2\text{O}_7$ samples were characterized by dc magnetic susceptibility, and these results are summarized in Table I. In each case, the transition to the ordered phase is marked by a cusp and a bifurcation of the field cooled and zero field cooled susceptibilities, as shown in the Supplemental Material [38]. Both the Néel temperature and the paramagnetic moment per formula unit systematically decrease as a function of the magnetic dilution. The Curie-Weiss temperature (θ_{CW}) does not vary appreciably in these three materials, ranging from $-17.2(3)$ K to $-18.0(2)$ K.

We performed time-of-flight elastic and inelastic neutron scattering on these three single crystals using the

Disc Chopper Spectrometer at the NIST Center for Neutron Research [39]. Measurements were performed in a dilution refrigerator in both zero magnetic field and an applied magnetic field along the $[1,-1,0]$ direction, perpendicular to the (HHL) scattering plane. For each of the three samples, magnetic Bragg peaks form below their respective Néel transitions (see Table I). The relative intensities of the magnetic Bragg reflections in the 10%-Y and 20%-Y crystals are unchanged from pure $\text{Er}_2\text{Ti}_2\text{O}_7$. That is to say, all three order into the Γ_5 irreducible representation, which is dominated by an intense magnetic Bragg reflection at (220) . In large magnetic fields, all three enter a field polarized state, characterized by an intense (111) magnetic Bragg reflection and the disappearance of the (220) magnetic reflection [40, 41].

The Γ_5 irreducible representation is comprised of two basis vectors, ψ_2 and ψ_3 , which are indistinguishable in an unpolarized elastic neutron scattering experiment. However, the distinction between ψ_2 and ψ_3 ground state selection can be resolved by considering the magnetic field dependence of the (220) magnetic Bragg peak. Both ψ_2 and ψ_3 display six distinct domains that are degenerate in zero field. This degeneracy is lifted by the application of a small magnetic field along the $[1,-1,0]$ direction, which selects out two of these six domains [20, 42, 43]. For ψ_2 , the two domains selected in a magnetic field are the ones that maximize the (220) magnetic Bragg peak, resulting in a twofold increase of its intensity. Conversely, for ψ_3 , the scenario is the opposite where the two domains selected in a field are the ones that give the smallest contribution to the (220) magnetic Bragg peak. We note these domain effects occur in small $[1,-1,0]$ fields, significantly below the onset of the field polarized state. The effect of the canting angle on the (220) Bragg peak intensity have been well characterized for $\text{Er}_2\text{Ti}_2\text{O}_7$ [40, 41, 44] and little effect is seen on its intensity between 0.1T and 1T. Hence, we used a field of 0.5T to investigate domain effects, which, is sufficiently large to overcome pinning of domains by disorder in a small field.

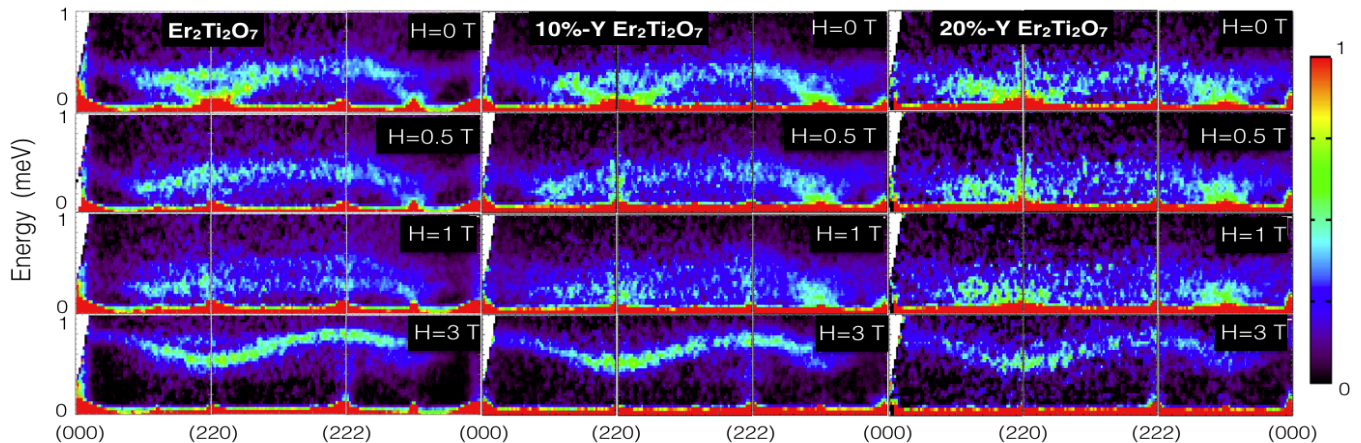


FIG. 2. Spin wave spectra along three different directions in the HHL plane: [HH0], [22L], and [HHH], all at $T = 0.1$ K. The spectra are shown for each of the three samples in zero magnetic field, and with magnetic fields of 0.5 T, 1 T, and 3 T applied along the [1-10] direction. The contour plots along the [HH0], [22L] and [HHH] directions are obtained by integrating the 3D data set, $S(\vec{Q}, E)$, over $-0.2 \leq [00L] \leq 0.2$, $1.8 \leq [HH0] \leq 2.2$ and $0.2 \leq [HH - 2H] \leq 0.2$, respectively.

Knowing how to distinguish ψ_2 from ψ_3 , we can now test the two theoretical predictions that magnetic dilution should induce a transition from ψ_2 to ψ_3 [36, 37]. Accordingly, we first consider the elastic scattering from the three crystals at the (220) Bragg position in zero field, 0.5 T and 3 T, as shown in Fig. 1. The intensities have been normalized using the Bragg intensity at $H = 3$ T, which corresponds to the polarized state where the scattered intensity at (220) is purely structural. As the field is increased to 0.5 T, we observe a marked increase in the peak intensity for the pure sample as well as for the 10%-Y doped sample, but not for the 20%-Y diluted crystal. More striking is the evolution of the shape of the (220) Bragg peak with magnetic dilution. In zero field, the undoped sample exhibits a resolution-limited Bragg peak with a small amount of diffuse scattering extending out along [HH0] (Fig. 1(a)). Upon dilution, the relative contribution of the resolution-limited Bragg scattering weakens with a corresponding increase in the diffuse scattering, such that the lineshape of the 20%-Y sample is dominated by a Lorentzian form in both zero field and at 0.5 T (Fig. 1(c)).

To determine the origin of the diffuse scattering around (220), we look to the full inelastic neutron spectra in Fig. 2. These data are shown along three reciprocal space directions for each of the three samples in four different magnetic fields applied along the [1,-1,0] direction. In zero field (top row of Fig. 2), the spin waves of the three samples are qualitatively similar, consisting of one flat branch near 0.4 meV and quasi-Goldstone modes which soften at (111) and (220). A previous high resolution inelastic neutron scattering study of the pure sample determined that the quasi-Goldstone modes are gapped by 0.053 ± 0.006 meV [28]. As the energy resolution associated with the present inelastic measurements is 0.09

meV, elastic cuts of the form shown in Fig. 1 necessarily integrate over some of the spectral weight of these quasi-Goldstone modes. Thus, for the pure sample, this low energy inelastic scattering is the origin of the diffuse scattering observed in our cuts over (220) in Fig. 1. However for the 10%-Y and especially the 20%-Y sample, our data suggests that the spin gap is reduced from 0.053 meV, allowing for additional quasi-elastic and elastic magnetic scattering, characteristic of a frozen mosaic of ψ_2 and ψ_3 domains.

In order to understand the contributions to the scattering in the cuts of Fig. 1, we fit each elastic data set to the sum of a Gaussian and a Lorentzian lineshape, quantifying the magnetic long-range order (LRO) and the dynamic, quasi-elastic or frozen spin contributions, respectively. An example of such a fit for each sample is shown in the Supplemental Material [38]. The resulting fits show that the relative contribution of the diffuse, Lorentzian lineshape grows as a function of doping and accounts for $\sim 75\%$ of the Q -integrated scattering near (220) in the 20%-Y sample at $T = 0.1$ K and zero field. We therefore suggest that with increasing magnetic dilution, x , the spin excitations near (220) in $\text{Er}_{2-x}\text{Y}_x\text{Ti}_2\text{O}_7$ soften to lower energies and freeze. This is likely the result of a collapsing spin gap, a direct measure of the selection of ψ_2 over ψ_3 .

We can now isolate the LRO component of the elastic scattering and study its field dependence at $T = 0.1$ K. Once again, we use the fits to the scattering around (220), wherein a resolution-limited Gaussian lineshape represents the LRO and a broadened Lorentzian represents the dynamic, quasi-elastic and frozen spin response captured by our finite energy resolution. The LRO integrated intensity at (220) is shown as a function of a [1,-1,0] magnetic field for each sample in the insets of Fig. 1.

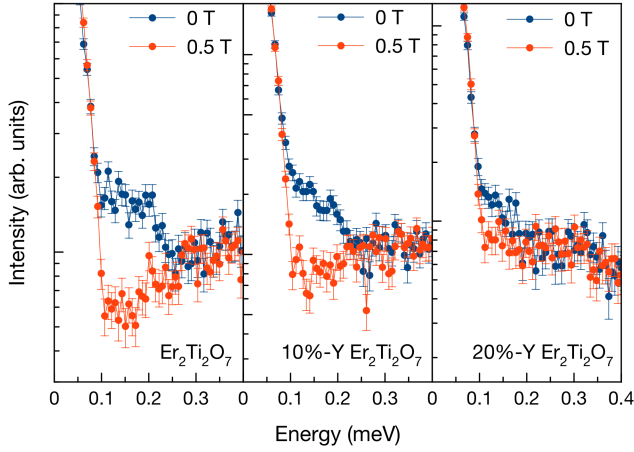


FIG. 3. Inelastic intensity as a function of energy at the (220) Bragg position for the pure, 10%-Y and 20%-Y diluted samples of $\text{Er}_{2-x}\text{Y}_x\text{Ti}_2\text{O}_7$. These plots are obtained by integrating the 3D data sets $S(\vec{Q}, E)$ at $T = 0.1$ K over $1.6 \leq [HH0] \leq 2.4$ and $-0.5 \leq [00L] \leq 0.5$.

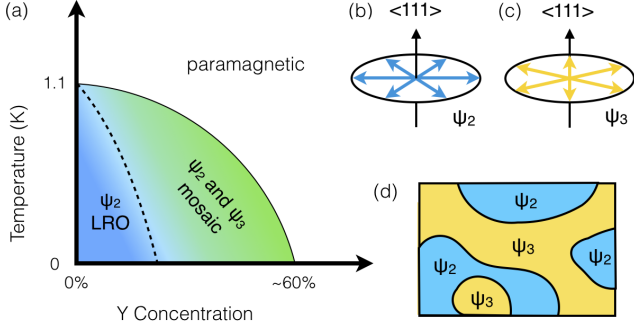


FIG. 4. (a) The schematic temperature-dilution phase diagram for $\text{Er}_{2-x}\text{Y}_x\text{Ti}_2\text{O}_7$. A dilution between 10%-Y and 20%-Y marks a crossover from a pure ψ_2 state into a frozen mosaic of ψ_2 and ψ_3 domains. The six discrete domains allowed by (b) ψ_2 and (c) ψ_3 within the XY plane. (d) Schematic illustration of the state at moderate dilution showing the mosaic of ψ_2 and ψ_3 domains.

Comparing the LRO intensity at zero field and 0.5 T, we observe a twofold increase for both the pure and 10%-Y samples, while the LRO is unchanged for the 20%-Y sample. This is a clear indication, via the domain selection scenario described above, that the pure and 10%-Y samples order into ψ_2 , but the 20%-Y sample does not. Furthermore, it is clear that these results are inconsistent with the detailed theoretical predictions that low levels of magnetic dilution should induce a transition from ψ_2 to ψ_3 [36, 37]. Indeed, neither the 10%-Y or 20%-Y samples order into ψ_3 as would be evidenced by an abrupt decrease of the (220) elastic intensity at $H = 0.5$ T.

A striking feature of Fig. 1, is the almost complete absence of diffuse scattering around (220) at $H = 0.5$ T for both the pure and 10%-Y samples, but not the 20%-Y

sample. Examination of the detailed spin wave spectra in Fig. 2, shows that a 0.5 T field gaps the quasi-Goldstone mode at (220) in the pure and 10%-Y samples (second row of Fig. 2). Meanwhile, quasi-elastic scattering persists around (220) in the 20%-Y sample to fields greater than 1 T. To quantify this effect, we integrated a small portion of reciprocal space around (220) and plotted the energy dependence of this scattering in zero field and 0.5 T for all three samples (Fig. 3). It is clear that the quasi-elastic scattering from the quasi-Goldstone modes in the pure and 10%-Y samples are gapped by ~ 0.3 meV in a 0.5 T field. However, for the 20%-Y sample, the zero field excitations are soft and the application of a 0.5 T magnetic field makes little difference to the low energy spectral weight near (220). Both of these observations are consistent with the absence of a spin wave gap and the associated domain selection in a magnetic field in the 20%-Y sample.

We propose the schematic phase diagram shown in Fig. 4 to describe the magnetic state in magnetically diluted $\text{Er}_{2-x}\text{Y}_x\text{Ti}_2\text{O}_7$. The phase transition and ψ_2 ground state selection are already well-established in the pure material [12, 16], along with the concomitant opening of a 0.053 ± 0.006 meV spin wave gap at $T_N = 1.1$ K [28]. Heat capacity measurements as a function of magnetic dilution are consistent with conventional 3D percolation theory [45], and a percolation threshold near 60%-Y has also been established [35]. The present measurements on magnetically diluted single crystal samples shows that ψ_2 domain selection is observed at low temperatures for the 10%-Y sample but not for the 20%-Y sample. This strongly suggests the presence of a phase boundary that mirrors the collapse of the spin gap as a function of dilution, indicated by the dashed line in Fig. 4(a). Weak dilution to the left of the dashed line produces a stable set of ψ_2 domains (Fig. 4(b)), at least above our minimum $T = 0.1$ K. However, to the right of the dashed line, the spin gap collapses and there is no mechanism for selection of ψ_2 over ψ_3 . A ground state characterized by a linear combination of ψ_2 and ψ_3 forming the full U(1) manifold is consistent with our data. However, in light of the theoretical study of ref [36, 37], it is then natural to think of the diluted system forming a frozen mosaic of ψ_2 and ψ_3 domains, with the ψ_3 domains (Fig. 4(c)) pinned by locally high concentrations of the quenched vacancies (Fig. 4(d)). It is interesting to note that a similar mixed ψ_2 and ψ_3 state is also observed in $\text{NaCaCo}_2\text{F}_7$ but believed to originate from bond disorder [46].

We find no evidence for the theoretically-predicted transition between the ψ_2 and ψ_3 ordered states in the presence of magnetic vacancies in $\text{Er}_{2-x}\text{Y}_x\text{Ti}_2\text{O}_7$. Measurements as a function of temperature in our most magnetically dilute sample, 20%-Y, provides no evidence for an additional phase transition between $T_N = 0.74(8)$ K and our base temperature of 0.1 K, as shown in Fig. 3 of

the Supplemental Material [38]. Nonetheless, we do identify a change in phase behavior between ψ_2 and a ground state characterized by no selection of ψ_2 over ψ_3 , likely a frozen mosaic of the two, all at dilution concentrations far below the 3D percolation threshold. Clearly, the preceding theoretical work correctly identified the sensitivity of the ψ_2 ground state selection to the presence of this form of quenched disorder, if not the detailed manifestation of the disorder on the phase behavior. As such, we hope our characterization of the spin statics and dynamics in single crystal $\text{Er}_{2-x}\text{Y}_x\text{Ti}_2\text{O}_7$, and low temperature phase behavior as a function of dilution, will motivate a complete understanding of these exotic, and fragile, ordered states.

We wish to acknowledge useful conversations with Leon Balents, Kate Ross, Mike Zhitomirsky, Michel Gingras, and Jeff Rau. We would also like to thank Juscelino Leao for his assistance with the sample environment. This work was supported by the Natural Sciences and Engineering Research Council of Canada and the Canada Foundation for Innovation. Work at the NIST Center for Neutron Research is supported in part by the National Science Foundation under Agreement No. DMR-0944772.

-
- [1] J. S. Gardner, M. J. P. Gingras, and J. E. Greedan, *Rev. Mod. Phys.* **82**, 53 (2010).
 - [2] M. J. Harris, S. T. Bramwell, D. F. McMorrow, T. H. Zeiske, and K. W. Godfrey, *Phys. Rev. Lett.* **79**, 2554 (1997).
 - [3] A. P. Ramirez, A. Hayashi, R. J. Cava, R. Siddharthan, and B. S. Shastry, *Nature* **399**, 333 (1999).
 - [4] C. Castelnovo, R. Moessner, and S. L. Sondhi, *Nature* **451**, 42 (2008).
 - [5] K. A. Ross, L. Savary, B. D. Gaulin, and L. Balents, *Phys. Rev. X* **1**, 021002 (2011).
 - [6] M. J. P. Gingras and P. A. McClarty, *Rep. Prog. Phys.* **77**, 056501 (2014).
 - [7] R. Applegate, N. R. Hayre, R. R. P. Singh, T. Lin, A. G. R. Day, and M. J. P. Gingras, *Phys. Rev. Lett.* **109**, 097205 (2012).
 - [8] S. Lee, S. Onoda, and L. Balents, *Phys. Rev. B* **86**, 104412 (2012).
 - [9] J. S. Gardner, S. R. Dunsiger, B. D. Gaulin, M. J. P. Gingras, J. E. Greedan, R. F. Kiefl, M. D. Lumsden, W. A. MacFarlane, N. P. Raju, J. E. Sonier, E. Swainson, and Z. Tun, *Phys. Rev. Lett.* **82**, 1012 (1999).
 - [10] H. Takatsu, H. Kadowaki, T. J. Sato, J. W. Lynn, Y. Tabata, T. Yamazaki, and K. Matsuhiro, *J. Phys. Condens. Matter* **24**, 052201 (2011).
 - [11] M. J. P. Gingras, B. C. Den Hertog, M. Faucher, J. S. Gardner, S. R. Dunsiger, L. J. Chang, B. D. Gaulin, N. P. Raju, and J. E. Greedan, *Phys. Rev. B* **62**, 6496 (2000).
 - [12] J. D. M. Champion, M. J. Harris, P. C. W. Holdsworth, A. S. Wills, G. Balakrishnan, S. T. Bramwell, E. Čížmár, T. Fennell, J. S. Gardner, J. Lago, D. F. McMorrow, M. Orendáč, A. Orendáčová, D. M. Paul, R. I. Smith, M. T. F. Telling, and A. Wildes, *Phys. Rev. B* **68**, 020401 (2003).
 - [13] H. Cao, A. Gukasov, I. Mirebeau, P. Bonville, C. Decorse, and G. Dhalenne, *Phys. Rev. Lett.* **103**, 056402 (2009).
 - [14] P. Bonville, S. Petit, I. Mirebeau, J. Robert, E. Lhotel, and C. Paulsen, *J. Phys. Condens. Matter* **25**, 275601 (2013).
 - [15] A. Bertin, Y. Chapuis, P. D. de Réotier, and A. Yaouanc, *J. Phys. Condens. Matter* **24**, 256003 (2012).
 - [16] A. Poole, A. S. Wills, and E. Lelievre-Berna, *J. Phys. Condens. Matter* **19**, 452201 (2007).
 - [17] J. Lago, T. Lancaster, S. J. Blundell, S. T. Bramwell, F. L. Pratt, M. Shirai, and C. Baines, *J. Phys. Condens. Matter* **17**, 979 (2005).
 - [18] P. Dalmas de Réotier, A. Yaouanc, Y. Chapuis, S. Curnoe, B. Grenier, E. Ressouche, C. Marin, J. Lago, C. Baines, and S. Giblin, *Phys. Rev. B* **86**, 104424 (2012).
 - [19] H. W. J. Blöte, R. F. Wielinga, and W. J. Huiskamp, *Physica* **43**, 549 (1969).
 - [20] L. Savary, K. A. Ross, B. D. Gaulin, J. P. C. Ruff, and L. Balents, *Phys. Rev. Lett.* **109**, 167201 (2012).
 - [21] S. Petit, J. Robert, S. Guitteny, P. Bonville, C. Decorse, J. Ollivier, H. Mutka, M. J. P. Gingras, and I. Mirebeau, *Phys. Rev. B* **90**, 060410 (2014).
 - [22] M. E. Zhitomirsky, M. V. Gvozdkova, P. C. W. Holdsworth, and R. Moessner, *Phys. Rev. Lett.* **109**, 077204 (2012).
 - [23] A. W. Wong, Z. Hao, and M. J. P. Gingras, *Phys. Rev. B* **88**, 144402 (2013).
 - [24] J. Oitmaa, R. R. P. Singh, B. Javanparast, A. G. R. Day, B. V. Bagheri, and M. J. P. Gingras, *Phys. Rev. B* **88**, 220404 (2013).
 - [25] M. E. Zhitomirsky, P. C. W. Holdsworth, and R. Moessner, *Phys. Rev. B* **89**, 140403 (2014).
 - [26] B. Javanparast, A. G. Day, Z. Hao, and M. J. P. Gingras, *Phys. Rev. B* **91**, 174424 (2015).
 - [27] P. A. McClarty, P. Stasiak, and M. J. P. Gingras, *Phys. Rev. B* **89**, 024425 (2014).
 - [28] K. A. Ross, Y. Qiu, J. R. D. Copley, H. A. Dabkowska, and B. D. Gaulin, *Phys. Rev. Lett.* **112**, 057201 (2014).
 - [29] J. G. Rau, S. Petit, and M. J. P. Gingras, *Phys. Rev. B* **93**, 184408 (2016).
 - [30] K. A. Ross, T. Proffen, H. A. Dabkowska, J. A. Quilliam, L. R. Yaraskavitch, J. B. Kycia, and B. D. Gaulin, *Phys. Rev. B* **86**, 174424 (2012).
 - [31] J. Gaudet, D. D. Maharaj, G. Sala, E. Kermarrec, K. A. Ross, H. A. Dabkowska, A. I. Kolesnikov, G. E. Granroth, and B. D. Gaulin, *Phys. Rev. B* **92**, 134420 (2015).
 - [32] A. Yaouanc, P. Dalmas de Réotier, C. Marin, and V. Glazkov, *Phys. Rev. B* **84**, 172408 (2011).
 - [33] T. Taniguchi, H. Kadowaki, H. Takatsu, B. Fåk, J. Ollivier, T. Yamazaki, T. J. Sato, H. Yoshizawa, Y. Shimura, T. Sakakibara, T. Hong, K. Goto, L. R. Yaraskavitch, and J. B. Kycia, *Phys. Rev. B* **87**, 060408 (2013).
 - [34] E. Kermarrec, D. D. Maharaj, J. Gaudet, K. Fritsch, D. Pomaranski, J. B. Kycia, Y. Qiu, J. R. D. Copley, M. M. P. Couchman, A. O. R. Morningstar, H. A. Dabkowska, and B. D. Gaulin, *Phys. Rev. B* **92**, 245114 (2015).
 - [35] J. F. Niven, M. B. Johnson, A. Bourque, P. J. Murray, D. D. James, H. A. Dabkowska, B. D. Gaulin, and M. A.

- White, in *Proc. R. Soc. A*, Vol. 470 (The Royal Society, 2014) p. 20140387.
- [36] V. S. Maryasin and M. E. Zhitomirsky, *Phys. Rev. B* **90**, 094412 (2014).
 - [37] A. Andreanov and P. A. McClarty, *Phys. Rev. B* **91**, 064401 (2015).
 - [38] The full susceptibility data and additionnal details on fitting of the magnetic Bragg peaks are shown in the Supplemental Material.
 - [39] J. R. D. Copley and J. C. Cook, *Chem. Phys.* **292**, 477 (2003).
 - [40] J. P. C. Ruff, J. P. Clancy, A. Bourque, M. A. White, M. Ramazanoglu, J. S. Gardner, Y. Qiu, J. R. D. Copley, M. B. Johnson, H. A. Dabkowska, *et al.*, *Phys. Rev. Lett.* **101**, 147205 (2008).
 - [41] P. A. McClarty, S. H. Curnoe, and M. J. P. Gingras, *J. Phys. Condens. Matter* **145**, 012032 (2009).
 - [42] Z. L. Dun, X. Li, R. S. Freitas, E. Arrighi, C. R. D. Cruz, M. Lee, E. S. Choi, H. B. Cao, H. J. Silverstein, C. R. Wiebe, *et al.*, *Phys. Rev. B* **92**, 140407 (2015).
 - [43] V. Maryasin, M. Zhitomirsky, and R. Moessner, *Phys. Rev. B* **93**, 100406 (2016).
 - [44] H. Cao, I. Mirebeau, A. Gukasov, P. Bonville, and C. Decorse, *Phys. Rev. B* **82**, 104431 (2010).
 - [45] B. D. Gaulin and J. S. Gardner, Chapter 8 : experimental studies of frustrated pyrochlore antiferromagnets in *Frustrated spin systems*, Singapore : World Scientific , 457 (2004).
 - [46] K. A. Ross, J. W. Krizan, J. A. Rodriguez-Rivera, R. J. Cava, and C. L. Broholm, *Phys. Rev. B* **93**, 014433 (2016).